# Improved Inkjet-Printed Pattern Fidelity: Suppressing Bulges by Segmented and Symmetric Drop Placement

**Ragheb Abunahla**
Department of Electrical Engineering and Computer Science
York University
4700 Keele St, EECS LAS 1012M
Toronto, ON, M3J 1P3, Canada
abunahlr@yorku.ca

**Md Saifur Rahman**
Department of Electrical Engineering and Computer Science
York University
4700 Keele St, EECS LAS 1012M
Toronto, ON, M3J 1P3, Canada
saifur29@eecs.yorku.ca

**Paria Naderi**
Department of Electrical Engineering and Computer Science
York University
4700 Keele St, EECS LAS 1012M
Toronto, ON, M3J 1P3, Canada
panaderi@eecs.yorku.ca

**Gerd Grau** [1]
Department of Electrical Engineering and Computer Science
York University
4700 Keele St, EECS LAS 1012M
Toronto, ON, M3J 1P3, Canada
grau@eecs.yorku.ca

**KEYWORDS:** micro-processing, printed electronics, inkjet printing, line morphology, bulging, scalloping, metal nanoparticle ink

[1] Corresponding author.

**ABSTRACT**

Inkjet printing is a promising technique for printed microelectronics due to low cost, customizability and compatibility with large-area, flexible substrates. However, printed line shapes can suffer from bulges at the start of lines and at corner points in 2D line patterns. The printed pattern can be multiple times wider than the designed linewidth. This can severely impact manufacturing accuracy and achievable circuit density. Bulging can be difficult to prevent without changing the ink-substrate-system, the drying conditions or the circuit design, all of which can be undesirable. Here, we demonstrate a novel printing methodology that solves this issue by changing the order in which drops are placed on the substrate. The pattern is split up into segments of three drops where the central drop is printed last. This symmetric printing prevents the unwanted ink flow that causes bulging. Larger bulge-free patterns are created by successively connecting segments. Line formation in both traditional linear printing and our novel segmented and symmetric printing was analyzed to understand and optimize results. The printing of X-, T- and L-shapes is considerably improved compared with the traditional linear printing methodology.

**INTRODUCTION**

Printed electronics is a promising new paradigm for the low-cost manufacturing of microelectronics [1–3] especially on large-area flexible substrates such as plastic and paper [4,5]. A range of devices have been printed including passive components [6], antennas [7], transistors [8–10], organic LEDs [11] and sensors [12,13] for applications such as RFID tags [14], flexible displays [15] and large-area sensing [16]. In particular, micro-inkjet printing is a common technique that allows designs to be customized on-the-

fly. A wide range of functional materials can be printed including conductors, insulators and semiconductors. Inkjet printing deposits ink droplets on a substrate that are ejected from a nozzle, typically using piezoelectric actuation (see Fig. 1). Ink droplets on the substrate coalesce to form a continuous pattern before the solvent dries off. Several subprocesses of the inkjet process have been studied and optimized. The interaction between the ink and the nozzle is crucial to achieve stable drop formation and jetting. Many studies have focused on nozzle design, waveform parameters and ink formulation [17–25]. However, in this work we focus on pattern formation after drops have been deposited on the substrate. Various patterns have been studied in the past including lines [26–32], rectangles [33–35] and more complex 2D patterns [36–38]. A commonly observed non-ideality in inkjet-printed line patterns is bulging. Large ink bulges can form at the beginning of lines or at intermediate positions along lines locally increasing linewidth potentially to multiple times the intended linewidth. Bulging at intermediate locations along straight lines can be solved by increasing the spacing between drops [28–30].

However, bulges at the beginning of lines have not been solved satisfactorily yet. Duinevald explains that bulging forms at the very start of the line when droplets merge due to cohesive forces [26]. As they merge, they form an ellipsoid shape rather than an elongated line to minimize surface energy. This ellipsoid forms the basis for the bulge at the beginning of a line. Droplets of spherical shape smaller than the bulge are continuously added to the front of the leading bead of the line. The difference in shape between the start and the leading edge of the line creates a pressure imbalance within the line due to differences in Laplace pressure. This pressure gradient creates a flow of liquid

from the front end of the line to the back of the line, where a bulge is being formed. As droplets are being added, the bulge expands, further lowering its pressure and driving ink towards it. As the line grows, resistance to flow increases eventually stopping growth of the bulge at the start of the line with a new bulge potentially being formed at the leading edge of the line. This process is illustrated in Fig. 2. This process has been observed not only for the starting point of simple lines but also at corners in 2D line patterns such as L-, T- and X-shapes [3,38,39]. This is the case because, for example, the second leg of an L-shape can be understood as the start of a new line with the opportunity for a bulge to form as described above. One reported remedy for this problem is an increase in print speed i.e. decreasing the time for unwanted flow in between deposition of subsequent droplets [26,31] but print speed cannot always be increased sufficiently as observed for the ink-substrate system here. Unwanted flow can also be suppressed by immediately solidifying each drop before the next drop is printed. This can be achieved by printing on a heated substrate, by immediately UV curing a UV curable ink or by interleaving drops with the first set of drops dried before the next set is printed. Without careful control, these methods can lead to a coin stacked morphology, which is undesirable for microelectronics, especially multi-layer devices, due to excessive roughness [28]. Without changing the ink-substrate-system [32], the only other reported remedies for this problem require the printed shapes to be changed. A guiding droplet has been printed next to the starting point of lines to divert the bulge to this side and keep a transistor channel clear [40]. A similar strategy has been applied to 2D line shapes by printing an anchoring structure at the beginning of the desired pattern to absorb the bulge [38]. Printing of wider lines, not single but multiple droplets wide, has also been shown to

remove bulging [38,39]. These solutions work in certain situations but are not general and limit the devices and circuits that can be printed. Here, we demonstrate a novel general method that removes bulges from the beginning of lines and corners in 2D line patterns for three ink-substrate-systems that otherwise exhibit bulging.

We recognize that the cause for bulging is a pressure imbalance within a line. Here, this pressure imbalance and thus bulging is prevented by changing the order in which drops are placed. Traditionally, drops are placed in a linear fashion from the start of the line to the end. We break this up by subdividing the line into smaller segments that are successively connected together. Every time segments are connected, it is ensured that both sides have the same pressure and therefore no bulges form due to pressure imbalances. The smallest segment consists of three droplets. First, the two outer droplets are printed and then connected by the third droplet at the center. There is no net force on this last center droplet due to the symmetry of the segment. Subsequently, multiple such segments are connected together using a connecting droplet without creating new pressure imbalances. The method is illustrated in Fig. 3. This segmented and symmetric printing methodology is similar to drop interleaving and can therefore be implemented with current printing technology; however, drops are not dried between passes, which can lead to coin stacking, and drop placement order and spacing are chosen carefully to avoid unwanted flow. This methodology allows us to print lines and 2D line shapes (L, T and X) without bulging.

## METHODS

### Equipment, Materials and Processes

A custom-built inkjet printer is used to deposit ink droplets on the substrate. The printer features independent x- and y-stages that allow vectorized motion of the substrate relative to the printhead. Any sequence of drop positions can be freely programmed using a custom LabView program. The printhead is a piezoelectric nozzle purchased from Microfab Technologies Inc. with a 60$\mu$m orifice diameter (MJ-ATP-01-060). We studied three different ink-substrate systems with two different representative inks (one conductor, one dielectric) on three different substrates (two different glass substrates, one polymer). The conductor ink was a commercial silver nanoparticle ink (ANP DGP 40LT-15C) with particle size of 35nm, viscosity of 16cP and tri(ethylene glycol) monoethyl ether as the major solvent. The dielectric ink was poly-4-vinylphenol (PVP), which is a commonly used polymer dielectric in printed electronics [41–44]. PVP was dissolved in 1-hexanol with a viscosity of 10cP. The solvents of both inks have a low vapor pressure at room temperature ensuring stable jetting without ink drying in the nozzle. The low vapor pressure ensures that the printed ink on the substrate has sufficient time to flow and reach its equilibrium state before drying. This also avoids the coin stacked morphology where ink dries sufficiently fast to avoid any flow but resulting surface roughness can be undesirable for microelectronic devices. Therefore, drying effects did not need to be taken into account when analyzing the flow that led to the final patterns. It was confirmed that all ink flow had terminated before recording optical micrographs of the final patterns by observing the ink flow with an angled camera during and immediately following printing. Inks were subsequently dried for 30 minutes on a hotplate at 150°C (silver) and

210°C respectively (PVP). Chemicals were purchased from Sigma-Aldrich except for the silver ink, which was purchased directly from Advanced Nano Products Co. The two glass substrates were Corning® EAGLE XG® display glass and Fisherbrand™ microscope slides. The polymer substrate was prepared by spin coating PVP onto display glass and cross-linking with poly(melamine-co-formaldehyde) methylated at 210°C for 30 minutes on a hotplate. PVP is commonly used as a smoothing layer for printed electronics on low-cost substrates [5,45]. Glass slides were cleaned in an ultrasonic bath for 30 minutes each in acetone and isopropanol and blow-dried in between and afterwards. During printing, substrates were fixed in place on the stage using vacuum. Print speed was 100mm/s and no improvement in bulging was observed when the print speed was set to the maximum achievable speed of 300mm/s. Drop volume and velocity of the ink ejected from the nozzle were measured using a camera and a stroboscopic light source that was synchronized with the jetting frequency [46,47]. Stationary images of droplets were taken at different delay times as they leave the nozzle giving a drop velocity between 1 and 2m/s depending on ink and jetting conditions. Stroboscopic imaging also confirmed that stable jetting without random variations was achieved. The contact angle of the ink on the substrate was measured using the sessile drop method by jetting a large number of droplets and observing the spherical cap of liquid forming on the substrate with a sideview camera. The sessile drop was small enough (approximately 1mm diameter) to exclude the effect of gravity.

**Printing Methodology**

Two different printing methodologies were tested. Traditional linear printing of droplets was used as a baseline comparison. Droplets were placed with a drop spacing (DSp) that was constant within each line. Lines with different drop spacing values were printed to find the optimum spacing and verify theoretical calculations. The drop spacing was varied from 50$\mu$m to 120$\mu$m. Fig. 2 illustrates this linear printing methodology.

Symmetric printing followed the same experimental methods; however, the order droplets were placed in was changed. The smallest component of a symmetrically printed line is a three-drop segment. The first droplet is printed at location (0, 0). Move twice the drop spacing (DSp) away to print the second droplet at (2*DSp, 0) (printing in the x-direction). Move back a single unit of drop spacing to place the third droplet at the center between the two droplets at (DSp, 0). The newly added droplet placed in between the two existing droplets has no net force acting on it thereby preventing unwanted fluid flow. The symmetric printing of segments is illustrated in Fig. 3 (a). These three-drop segments are the basis of our segmented printing approach. Building on these segments, lines of greater length can be built following the same rules used to create the segments. Segments/droplets of equal volume are connected by printing a connecting droplet in between segments. An important parameter is the spacing between segments before they are connected together. This was termed the connecting drop spacing (CDSp) and defined as the center-to-center spacing between the outermost drop in a segment and the connecting drop (see Fig. 3 (b)). The same segmented printing can be applied to more complex two-dimensional shapes such as X-, L- and T-shapes (see Fig. 3 (c)). In this case, the individual legs of the shapes are printed using our segmented and symmetric

approach before they are connected together with another droplet at the corner point. In our test structures, each leg contains two segments of three drops each with the same DSp and CDSp found optimal for straight lines.

## RESULTS AND DISCUSSION

Table 1 summarizes the experimental results of characterizing droplets and ink-substrate-interface. Droplet radius was measured in the air on the way to the substrate after being ejected from the nozzle. The observed drop cross-section was circular without satellites and thus drop volume was calculated assuming a spherical drop shape. The drop radius of an isolated drop on the substrate after drying ($R_S$) was used to calculate the contact angle and it was confirmed that this value agrees well with the contact angle measured using the sessile drop method. These values were used in subsequent calculations to understand line formation and predict optimal drop spacing. $R_S$ was used to normalize geometrical quantities such as drop spacing and linewidth as is common in related work [27–32]. The non-dimensional drop spacing was defined as $y$=DSp/$R_S$. This characterization of the drops in the air and of the ink-substrate interface is crucial to understand and optimize the line formation process.

### Linear Printing

In order to serve as a benchmark and to study the effect of bulging in lines, PVP lines were first printed using the traditional linear drop placement method. Fig. 4 shows such lines for different values of drop spacing. One can clearly observe a bulge at the start of each line except for the largest drop spacing where the line starts to break up. This case of strong bulging in our ink-substrate system is illustrative of the bulging phenomenon. One

can also observe strong scalloping along the length of the line for large values of drop spacing. Some degree of scalloping persists all the way down to a drop spacing of 65$\mu$m, which is a relatively small drop spacing for this drop volume and contact angle corresponding to a normalized drop spacing $y$=0.93.

There are two main published theories to determine the maximum drop spacing in an inkjet-printed line above which scalloping occurs [27,28]. Both predict the width of the line by dividing drop volume by drop spacing to calculate the liquid volume per unit line length. This corresponds to the cross-sectional area of a line. The line width can be determined from this by correcting for contact angle ($\theta$) according to the following equation:

$$W_{line} = \sqrt{\frac{V_{drop}}{DSp\left(\frac{\theta}{\sin\ (\theta)^2} - \frac{1}{\tan(\theta)}\right)}} \quad (1)$$

Stringer et al [27] compare the predicted line width to the diameter of an isolated drop on the substrate. If the drop diameter is larger than the line width, scalloping is possible. In our system, this occurs at a normalized drop spacing $y$ of 1.2. Graphically in Fig. 5, this corresponds to the intersection of the predicted line width curve (solid line) and the horizontal line representing the isolated drop diameter on the substrate. However, we find that experimental line width (circles) never exceeds the isolated drop diameter for any drop spacing we tested. This is due to the fact that liquid is removed from the line as it flows to the bulge. This means Eq. (1) overestimates liquid volume per unit length and consequently line width when significant bulging is present. The prediction becomes accurate for large values of drop spacing where bulging is diminished. Soltman et al [28] consider the radius of the droplet after initial expansion when it makes contact with the

end of the line. The radius of this impinging drop is calculated by simple geometry assuming the line terminates with a semi-circular contact line of radius equal to half the linewidth:

$$R_{drop\ ,impinging} = DSp - \frac{W_{line}}{2} \quad (2)$$

Soltman found that stable lines without scalloping can occur when the impinging drop diameter is less than the linewidth and always occur when the radius of the impinging drop is less than zero i.e. when the drop lands directly on the existing line. The former condition occurs at a normalized drop spacing of 1.65 in our case, which is well inside the scalloping regime. Therefore, focusing on the latter condition yields a normalized drop spacing of 1.06 when using line width predicted by Eq. (1) in Eq. (2). However, we do still observe some minor scalloping for drop spacing less than 1.06. This is due to the reduced line width caused by the bulge at the start of the line (see Fig. 5 for illustration). If this is taken into account, the impinging drop radius crosses zero at a drop spacing of approximately 0.85. This is in good agreement with experimental results where we observe no scalloping for drop spacing of 0.86 and below. Fig. 5 shows the difference in calculated impinging drop radius when linewidth is predicted without taking into account bulging (dashed line) and using experimental linewidth (squares). Hsiao et al have also observed an underestimation of the impinging drop radius by Eq. (2), although in their case this was due to a combination of drop impact inertia and a non-pinned contact line [31]. The results presented here illustrate the interaction between the effects of scalloping and bulging, which can occur simultaneously. In such a case, varying drop spacing alone cannot create a smooth line without either bulges or scallops. In the next section, a novel segmented and symmetric drop placement approach is demonstrated that can achieve

smooth lines in such situations without changing substrate, ink, drying conditions or pattern.

**Symmetric Printing**

The key to solving the bulging issue is to not allow a bulge to form at the start of a line. Here, this is achieved by symmetrically printing segments of three drops i.e. depositing the outer two drops first before printing the central drop that connects them. Fig. 6 shows such three-drop PVP segments printed with different drop spacing. Segments exhibit bulging for small values of drop spacing up to 95$\mu$m ($y$=1.36). Segments become straight for larger values of drop spacing until the onset of scalloping can be observed at 120$\mu$m ($y$=1.71). Fig. 7 shows the experimental linewidth measured at the center of the segment for all three ink-substrate systems. The three different ink-substrate systems differ in terms of contact angle and drop volume leading to a different drop radius on the substrate. Once drop spacing and line width are normalized by $R_S$ (see Fig. 7 (b)), the three systems exhibit very similar behavior except the normalized linewidth increases slightly with decreasing contact angle. This leads to slightly different values of optimal drop spacing $y$= 1.3, 1.6 and 1.7 respectively for contact angles 43.4°, 23.4° and 17.5°. In order to predict these different regimes, one can calculate the width of the segment and compare it to the size of an isolated drop. By the time the third drop is added, the two outer drops have spread fully to the same extent as isolated drops because the time scale for drop spreading is microseconds [48] and the time between drop ejection is on the order of milliseconds. If the calculated linewidth is larger than the diameter of isolated drops, bulging will be observed. If the calculated linewidth is smaller than the diameter of isolated drops, scalloping will be observed. Linewidth calculated using Eq. (1) (dashed

line in Fig. 7) is significantly smaller than experimental values. Equation (1) assumes an infinitely long line without taking into account the effect of line termination. This is not the case for short three-drop line segments. The two ends of the segment exhibit additional curvature of the liquid surface. In order to maintain equilibrium and balance pressure with the straight center of the line segment, the liquid surface at the ends needs to deform from the spherical cap shape of an isolated drop. The equilibrium shape of three-drop segments was calculated using the open source software Surface Evolver. The results of this model (solid lines in Fig. 7) exhibit much better agreement with experiment than Eq. (1). The optimal drop spacing found for segments was subsequently used to print larger lines.

The final step to create larger line patterns is to connect the individual three-drop segments together by placing a connecting drop in between. If the same drop spacing is used for the connecting drop as for the segments, the average drop spacing will be too large to form a line without scalloping. In a long line, the average drop spacing is simply the mean between the drop spacing within segments (DSp) and the connecting drop spacing between segments (CDSp). In this situation, the assumptions of Stringer's model are a good representation i.e. a uniform semi-infinite line. Therefore, the average drop spacing should exhibit the same ideal value as predicted by Stringer (1.18 for PVP on glass). If the connecting drop spacing is the same as the segment drop spacing, the average drop spacing will be much larger (1.57). This leads to significant scalloping as observed in Fig. 8 (a). CDSp needs to be reduced to prevent this. The minimum value CDSp can take is the radius of the contact line at the end of each segment, which is approximately equal to the radius of an isolated drop on the substrate. If CDSp is reduced

further, segments will touch before they are connected by a connecting drop in a controlled fashion. This leads to unwanted bulging. Therefore, the minimum normalized CDSp is 1. The corresponding average drop spacing is 1.29, which is close to the ideal drop spacing. Fig. 8 (b) confirms that for all three ink-substrate systems lines printed with this minimum CDSp exhibit much reduced scalloping and no bulging as observed for linear printing.

The same segmented printing approach was applied to 2D X-, T- and L-line shapes. These shapes can be understood as a new line starting from the crossing point, which means bulging can occur. By printing each leg separately first and subsequently connecting them, there is no pressure imbalance that will cause bulging. Fig. 9 (a) shows X-, T- and L-shapes that were printed using the traditional linear methodology. One can observe both bulges at the beginning of legs and at the crossing point manifested as a convex contact line. In the case of the X-shape, the two bulges merged together. Conversely, shapes printed with the segmented approach do not exhibit bulging at the start of legs or the crossing point (see Fig. 9 (b)). One can still observe some corner rounding at the crossing point, which is due to surface energy minimization of the liquid ink. Surface energy minimization is the second mechanism that causes non-idealities in printed corners even when no bulging is present. It was not optimized here because our method focuses on bulges that lead to catastrophic pattern distortions such as those exhibited by X-shapes in Fig. 9 (a) (i). The size of the non-ideality is reduced and the contact line is concave confirming that the cause for the remaining non-ideality is surface energy minimization rather than bulging. The area of the non-ideality at the crossing was reduced by 75% for X-shapes, 32% for T-shapes and 34% for L-shapes. For X-shapes,

the bulge at the crossing and the bulge at the front of the right line have flown together. To estimate the area of the bulge at the crossing, the average area of a bulge at the front of a line was subtracted from the overall bulge area. If the bulges at the beginning of all lines are also considered, our method reduces the total non-ideality area by 85% for X-shapes, 61% for T-shapes and 65% for L-shapes respectively. Fig. 10 shows the effect of varying the spacing between legs in X-shapes. The range of possible values for the spacing is limited. If the spacing is too small, legs will touch before being connected in a controlled fashion. If the distance is too large, legs will not be connected by the connecting drop. One can observe a small reduction in corner rounding as the spacing between legs is increased but all X-shapes show similar behavior without bulging or scalloping.

## CONCLUSIONS

A novel drop placement methodology for inkjet-printed line patterns is presented. Traditional linear printing can lead to bulging at the start of lines and scalloping, which can occur simultaneously as demonstrated here. Line formation was studied for this case to understand the interaction between the two effects. It was found that bulging can promote scalloping. This is solved by changing the order in which droplets are placed on the substrate. First, segments of three drops are printed where the central drop is printed last. The symmetry in this structure prevents bulges from forming if the right drop spacing is chosen. Then, such segments are connected with another drop to form larger line patterns including X-, T- and L-shapes without bulges and with minimal scalloping. This is a considerable improvement over traditional linear printing. The method was

demonstrated and studied for three different ink-substrate systems. Future work could extend this to other ink-substrate systems including the effect of substrate roughness.

## FUNDING

We acknowledge the support of the Natural Sciences and Engineering Research Council of Canada (NSERC), funding reference number STPGP 521480-18, and of the Lassonde School of Engineering, York University (operating funds from G. Grau's start-up grant and funding for R. Abunahla from the Lassonde Undergraduate Research Award (LURA)).

## NOMENCLATURE

| | |
|---|---|
| DSp | Drop Spacing within linear lines and symmetrically printed segments |
| CDSp | Connecting Drop Spacing between symmetrically printed segments |
| $R_s$ | Drop radius on the substrate |
| $y$ | Drop spacing normalized by $R_S$ |
| $R_0$ | Drop radius in flight before hitting substrate |
| $V_{drop}$ | Drop volume |
| $\theta$ | Contact angle |
| $W_{line}$ | Linewidth |

## REFERENCES


[1] Arias, A. C., MacKenzie, J. D., McCulloch, I., Rivnay, J., and Salleo, A., 2010, "Materials and Applications for Large Area Electronics: Solution-Based Approaches," Chemical Reviews, **110**(1), pp. 3–24.

[2] Moonen, P. F., Yakimets, I., and Huskens, J., 2012, "Fabrication of Transistors on Flexible Substrates: From Mass-Printing to High-Resolution Alternative Lithography Strategies," Advanced Materials, **24**(41), pp. 5526–5541.

[3] Subramanian, V., Cen, J., de la Fuente Vornbrock, A., Grau, G., Kang, H., Kitsomboonloha, R., Soltman, D., and Tseng, H.-Y., 2015, "High-Speed Printing of Transistors: From Inks to Devices," Proceedings of the IEEE, **103**(4), pp. 567–582.

[4] Tobjörk, D., and Österbacka, R., 2011, "Paper Electronics," Advanced Materials, **23**, pp. 1935–1961.

[5] Grau, G., Kitsomboonloha, R., Swisher, S. L., Kang, H., and Subramanian, V., 2014, "Printed Transistors on Paper: Towards Smart Consumer Product Packaging," Advanced Functional Materials, **24**(32), pp. 5067–5074.

[6] McKerricher, G., Gonzalez Perez, J., and Shamim, A., 2015, "Fully Inkjet Printed RF Inductors and Capacitors Using Polymer Dielectric and Silver Conductive Ink With Through Vias," IEEE Transactions on Electron Devices, **62**(3), pp. 1002–1009.

[7] Cook, B. S., and Shamim, A., 2012, "Inkjet Printing of Novel Wideband and High Gain Antennas on Low-Cost Paper Substrate," IEEE Transactions on Antennas and Propagation, **60**(9), pp. 4148–4156.

[8] Sirringhaus, H., 2000, "High-Resolution Inkjet Printing of All-Polymer Transistor Circuits," Science, **290**(5499), pp. 2123–2126.

[9] Sekitani, T., Noguchi, Y., Zschieschang, U., Klauk, H., and Someya, T., 2008, "Organic Transistors Manufactured Using Inkjet Technology with Subfemtoliter Accuracy," Proceedings of the National Academy of Sciences, **105**(13), pp. 4976–4980.

[10] Grau, G., and Subramanian, V., 2016, "Fully High-Speed Gravure Printed, Low-Variability, High-Performance Organic Polymer Transistors with Sub-5V Operation," Advanced Electronic Materials, **2**(4).

[11] Tekoglu, S., Hernandez-Sosa, G., Kluge, E., Lemmer, U., and Mechau, N., 2013, "Gravure Printed Flexible Small-Molecule Organic Light Emitting Diodes," Organic Electronics, **14**(12), pp. 3493–3499.

[12] Chang, J. B., Liu, V., Subramanian, V., Sivula, K., Luscombe, C., Murphy, A., Liu, J., and Fréchet, J. M. J., 2006, "Printable Polythiophene Gas Sensor Array for Low-Cost Electronic Noses," J. Appl. Phys., **100**(1), p. 014506.

[13] Someya, T., Kato, Y., Sekitani, T., Iba, S., Noguchi, Y., Murase, Y., Kawaguchi, H., and Sakurai, T., 2005, "Conformable, Flexible, Large-Area Networks of Pressure and Thermal Sensors with Organic Transistor Active Matrixes," Proceedings of the National Academy of Sciences of the United States of America, **102**(35), pp. 12321–12325.

[14] Namsoo Lim, Jaeyoung Kim, Soojin Lee, Namyoung Kim, and Gyoujin Cho, 2009, "Screen Printed Resonant Tags for Electronic Article Surveillance Tags," Advanced

Packaging, IEEE Transactions on DOI - 10.1109/TADVP.2008.2006656, **32**(1), pp. 72–76.
[15] Sekitani, T., Nakajima, H., Maeda, H., Fukushima, T., Aida, T., Hata, K., and Someya, T., 2009, "Stretchable Active-Matrix Organic Light-Emitting Diode Display Using Printable Elastic Conductors," Nat Mater, **8**(6), pp. 494–499.
[16] Sekitani, T., Takamiya, M., Noguchi, Y., Nakano, S., Kato, Y., Sakurai, T., and Someya, T., 2007, "A Large-Area Wireless Power-Transmission Sheet Using Printed Organic Transistors and Plastic MEMS Switches," Nat Mater, **6**(6), pp. 413–417.
[17] Hoath, S. D., Hsiao, W.-K., Jung, S., Martin, G. D., Hutchings, I. M., Morrison, N. F., and Harlen, O. G., 2013, "Drop Speeds from Drop-on-Demand Ink-Jet Print Heads," Journal of Imaging Science and Technology, **57**(1), pp. 1–11.
[18] Nallan, H. C., Sadie, J. A., Kitsomboonloha, R., Volkman, S. K., and Subramanian, V., 2014, "Systematic Design of Jettable Nanoparticle-Based Inkjet Inks: Rheology, Acoustics, and Jettability," Langmuir, **30**(44), pp. 13470–13477.
[19] Liu, Y.-F., Tsai, M.-H., Pai, Y.-F., and Hwang, W.-S., 2013, "Control of Droplet Formation by Operating Waveform for Inks with Various Viscosities in Piezoelectric Inkjet Printing," Applied Physics A, **111**(2), pp. 509–516.
[20] Liu, Y., and Derby, B., 2019, "Experimental Study of the Parameters for Stable Drop-on-Demand Inkjet Performance," Physics of Fluids, **31**(3), p. 032004.
[21] Lai, J.-M., Huang, C.-Y., Chen, C.-H., Linliu, K., and Lin, J.-D., 2010, "Influence of Liquid Hydrophobicity and Nozzle Passage Curvature on Microfluidic Dynamics in a Drop Ejection Process," Journal of Micromechanics and Microengineering, **20**(1), p. 015033.
[22] Reis, N., Ainsley, C., and Derby, B., 2005, "Ink-Jet Delivery of Particle Suspensions by Piezoelectric Droplet Ejectors," Journal of Applied Physics, **97**(9), p. 094903.
[23] Yang, Q., Li, H., Li, M., Li, Y., Chen, S., Bao, B., and Song, Y., 2017, "Rayleigh Instability-Assisted Satellite Droplets Elimination in Inkjet Printing," ACS Applied Materials & Interfaces, **9**(47), pp. 41521–41528.
[24] Wu, H.-C., Shan, T.-R., Hwang, W.-S., and Lin, H.-J., 2004, "Study of Micro-Droplet Behavior for a Piezoelectric Inkjet Printing Device Using a Single Pulse Voltage Pattern," Materials Transactions, **45**(5), pp. 1794–1801.
[25] He, B., Yang, S., Qin, Z., Wen, B., and Zhang, C., 2017, "The Roles of Wettability and Surface Tension in Droplet Formation during Inkjet Printing," Scientific Reports, **7**(1).
[26] Duineveld, P. C., 2003, "The Stability of Ink-Jet Printed Lines of Liquid with Zero Receding Contact Angle on a Homogeneous Substrate," Journal of Fluid Mechanics, **477**.
[27] Stringer, J., and Derby, B., 2009, "Limits to Feature Size and Resolution in Ink Jet Printing," Journal of the European Ceramic Society, **29**(5), pp. 913–918.
[28] Soltman, D., and Subramanian, V., 2008, "Inkjet-Printed Line Morphologies and Temperature Control of the Coffee Ring Effect," Langmuir, **24**(5), pp. 2224–2231.
[29] Stringer, J., and Derby, B., 2010, "Formation and Stability of Lines Produced by Inkjet Printing," Langmuir, **26**(12), pp. 10365–10372.

[30] Oh, Y., Kim, J., Yoon, Y. J., Kim, H., Yoon, H. G., Lee, S.-N., and Kim, J., 2011, "Inkjet Printing of Al2O3 Dots, Lines, and Films: From Uniform Dots to Uniform Films," Current Applied Physics, **11**(3), pp. S359–S363.
[31] Hsiao, W.-K., Martin, G. D., and Hutchings, I. M., 2014, "Printing Stable Liquid Tracks on a Surface with Finite Receding Contact Angle," Langmuir, **30**(41), pp. 12447–12455.
[32] Du, Z., Xing, R., Cao, X., Yu, X., and Han, Y., 2017, "Symmetric and Uniform Coalescence of Ink-Jetting Printed Polyfluorene Ink Drops by Controlling the Droplet Spacing Distance and Ink Surface Tension/Viscosity Ratio," Polymer, **115**, pp. 45–51.
[33] Soltman, D., Smith, B., Kang, H., Morris, S. J. S., and Subramanian, V., 2010, "Methodology for Inkjet Printing of Partially Wetting Films," Langmuir, **26**(19), pp. 15686–15693.
[34] Kang, H., Soltman, D., and Subramanian, V., 2010, "Hydrostatic Optimization of Inkjet-Printed Films," Langmuir, **26**(13), pp. 11568–11573.
[35] Soltman, D., Smith, B., Morris, S. J. S., and Subramanian, V., 2013, "Inkjet Printing of Precisely Defined Features Using Contact-Angle Hysteresis," Journal of Colloid and Interface Science, **400**, pp. 135–139.
[36] Diaz, E., Ramon, E., and Carrabina, J., 2013, "Inkjet Patterning of Multiline Intersections for Wirings in Printed Electronics," Langmuir, **29**(40), pp. 12608–12614.
[37] Vila, F., Pallares, J., Ramon, E., and Teres, L., 2016, "A Systematic Study of Pattern Compensation Methods for All-Inkjet Printing Processes," IEEE Transactions on Components, Packaging and Manufacturing Technology, **6**(4), pp. 630–636.
[38] Chen, C.-T., and Hung, T.-Y., 2016, "Morphology and Deposit of Picoliter Droplet Tracks Generated by Inkjet Printing," Journal of Micromechanics and Microengineering, **26**(11), p. 115005.
[39] Jagannathan, L., 2012, "Organic and Printed Electronics for Biological Microfluidic Applications," PhD dissertation, University of California, Berkeley.
[40] de la Fuente Vornbrock, A., Sung, D., Kang, H., Kitsomboonloha, R., and Subramanian, V., 2010, "Fully Gravure and Ink-Jet Printed High Speed PBTTT Organic Thin Film Transistors," Organic Electronics, **11**(12), pp. 2037–2044.
[41] Facchetti, A., Yoon, M.-H., and Marks, T. J., 2005, "Gate Dielectrics for Organic Field-Effect Transistors: New Opportunities for Organic Electronics," Adv. Mater., **17**(14), pp. 1705–1725.
[42] Roberts, M. E., Queraltó, N., Mannsfeld, S. C. B., Reinecke, B. N., Knoll, W., and Bao, Z., 2009, "Cross-Linked Polymer Gate Dielectric Films for Low-Voltage Organic Transistors," Chemistry of Materials, **21**(11), pp. 2292–2299.
[43] Tseng, H.-Y., and Subramanian, V., 2011, "All Inkjet-Printed, Fully Self-Aligned Transistors for Low-Cost Circuit Applications," Organic Electronics, **12**(2), pp. 249–256.
[44] Kim, S. J., Jang, M., Yang, H. Y., Cho, J., Lim, H. S., Yang, H., and Lim, J. A., 2017, "Instantaneous Pulsed-Light Cross-Linking of a Polymer Gate Dielectric for Flexible Organic Thin-Film Transistors," ACS Applied Materials & Interfaces, **9**(13), pp. 11721–11731.

[45] Molesa, S. E., De La Fuente Vornbrock, A., Chang, P. C., and Subramanian, V., 2005, "Low-Voltage Inkjetted Organic Transistors for Printed RFID and Display Applications," *Technical Digest - International Electron Devices Meeting, IEDM*, IEEE, pp. 109–112.
[46] International Electrotechnical Commission (IEC), 2017, "IEC Standard 62899-302-1 Printed Electronics – Part 302-1: Equipment – Inkjet – Imaging Based Measurement of Jetting Speed."
[47] International Electrotechnical Commission (IEC), 2018, "IEC Standard 62899-302-2 Printed Electronics – Part 302-2: Equipment – Inkjet – Imaging-Based Measurement of Droplet Volume."
[48] Dong, H., Carr, W. W., Bucknall, D. G., and Morris, J. F., 2007, "Temporally-Resolved Inkjet Drop Impaction on Surfaces," AIChE Journal, **53**(10), pp. 2606–2617.

## Figure Captions List

Fig. 1: Illustration of the inkjet printing process

Fig. 2: Illustration of the generation of bulges in linear printing due to pressure driven flow as subsequent drops are added to a developing line

Fig. 3: Illustration of the segmented and symmetric printing methodology. (a) First, segments of three drops are printed by placing the central drop last. Due to the symmetry, bulging can be prevented. The most important parameter is the spacing between drops (DSp). (b) Second, three-drop segments are connected with a drop in between segments. The connecting drop spacing (CDSp) is different from DSp within segments. (c) Finally, longer lines or 2D patterns (e.g. X-shapes) are created by subsequently connecting more and more segments.

Fig. 4: PVP lines printed in a linear fashion with varying drop spacing. Bulging is clearly visible at the start of lines (top) with small drop spacing. Scalloping is also clearly visible for large values of drop spacing. The two regimes overlap. The only line without any bulging exhibits line separation (DSp=120$\mu$m). Scale bar represents 200$\mu$m.

Fig. 5: (a) Illustration of scalloping mechanism induced by bulging. (i) With a bulge at the start of the line, ink is removed from the line reducing linewidth. Newly added drops land outside of the existing line and spread before merging with the line leading to scalloping. (ii) Without bulge for the same drop spacing, linewidth is larger. New drops land directly on the existing line preventing scalloping. (b) Stability diagram to identify drop spacing below which no scalloping occurs. Both axes show dimensions normalized by *RS*. Stringer's model predicts this transition at the crossing point of the predicted line width (solid line) and the diameter of an isolated drop (horizontal line). However, experimental linewidth (circles) is less than the predicted value due to ink being removed to the bulge. Soltman's model considers where the diameter of impinging drops crosses zero as they make contact with the line. This gives good agreement with experimental values (transition at y=0.86) when the impinging diameter is calculated using experimental (squares) rather than predicted (dashed line) linewidth.

Fig. 6: Segments of three PVP drops printed symmetrically with varying drop spacing. Scale bar represents 200$\mu$m.

Fig. 7: Linewidth at the center of three-drop segments printed symmetrically as a function of drop spacing for three different ink-substrate systems. (a) absolute dimensions and (b) dimensions normalized by drop radius on substrate. Optimum drop spacing corresponds to segments with linewidth just above twice the drop radius (horizontal line in (b)).

Fig. 8: Symmetrically printed lines with two (left) and four (right) segments. No bulging is observed. (a) Connecting drop spacing between segments is the same as drop spacing within segments. (b) Connecting drop spacing is reduced to minimum, significantly

reducing scalloping. (i) PVP on glass. (ii) Silver on polymer. (iii) Silver on glass. Scale bar represents 200$\mu$m.

Fig. 9: X-, T- and L-shapes printed with (a) traditional linear method and (b) segmented and symmetric method without bulging. Insets illustrate printing methodologies. PVP on glass. Scale bar represents 200$\mu$m.

Fig. 10: X-shapes symmetrically printed with varying spacing between legs. The spacing between the center of the innermost drop in each segment and the center of the central connecting drop is (a) 110$\mu$m (b) 120$\mu$m (c) 130$\mu$m and (d) 140$\mu$m. PVP on glass. Scale bar represents 200$\mu$m.

## Table Caption List

Table 1: Measured properties of droplets in air after being ejected from nozzle and at interface with substrate

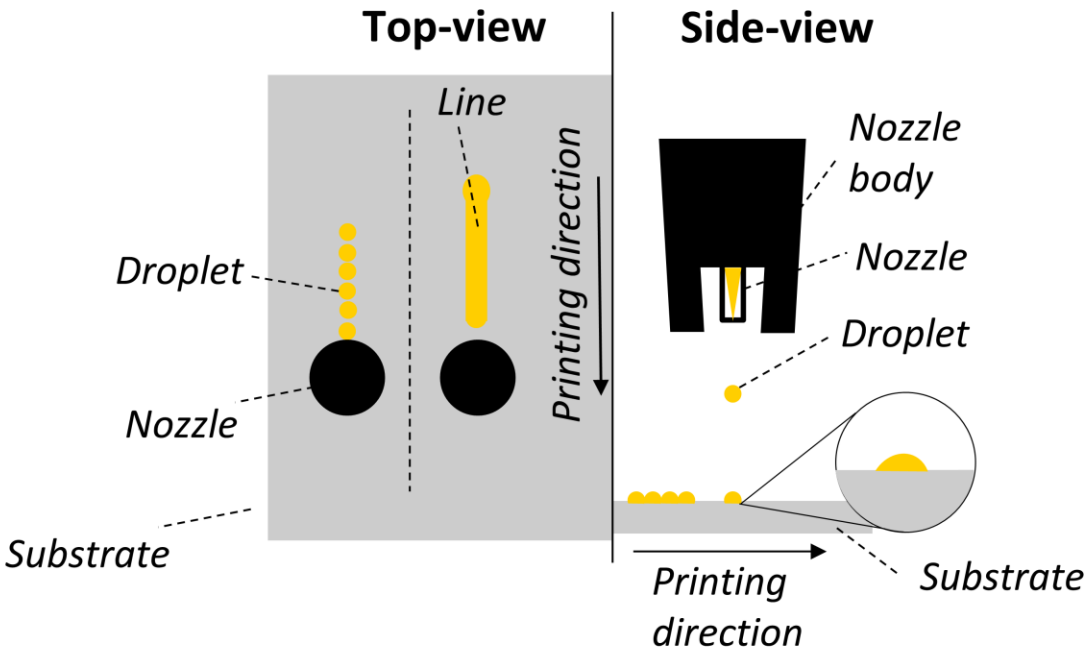


Fig. 1: Illustration of the inkjet printing process

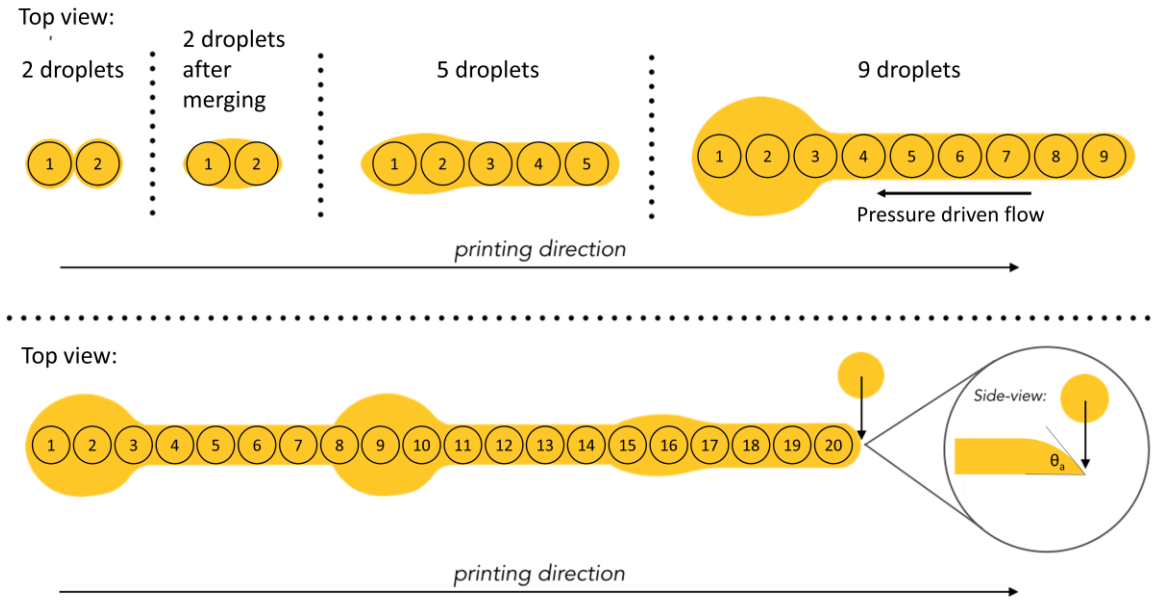


Fig. 2: Illustration of the generation of bulges in linear printing due to pressure driven flow as subsequent drops are added to a developing line

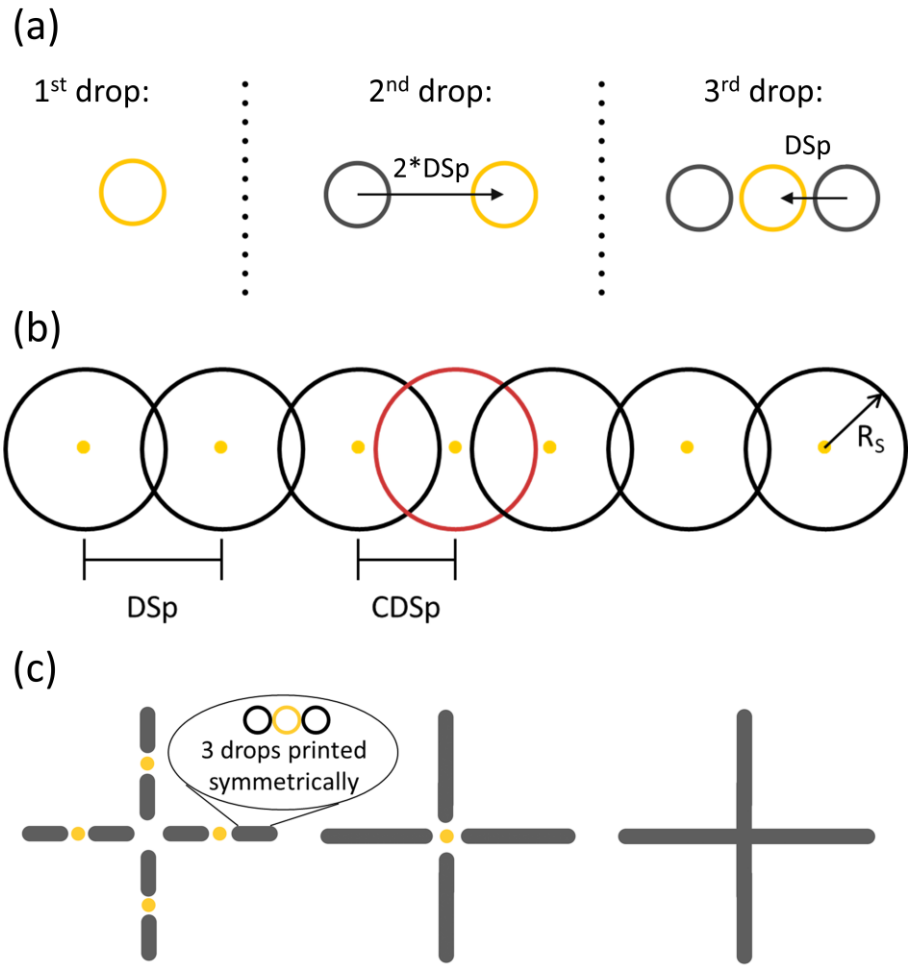


Fig. 3: Illustration of the segmented and symmetric printing methodology. (a) First, segments of three drops are printed by placing the central drop last. Due to the symmetry, bulging can be prevented. The most important parameter is the spacing between drops (DSp). (b) Second, three-drop segments are connected with a drop in between segments. The connecting drop spacing (CDSp) is different from DSp within segments. (c) Finally, longer lines or 2D patterns (e.g. X-shapes) are created by subsequently connecting more and more segments.

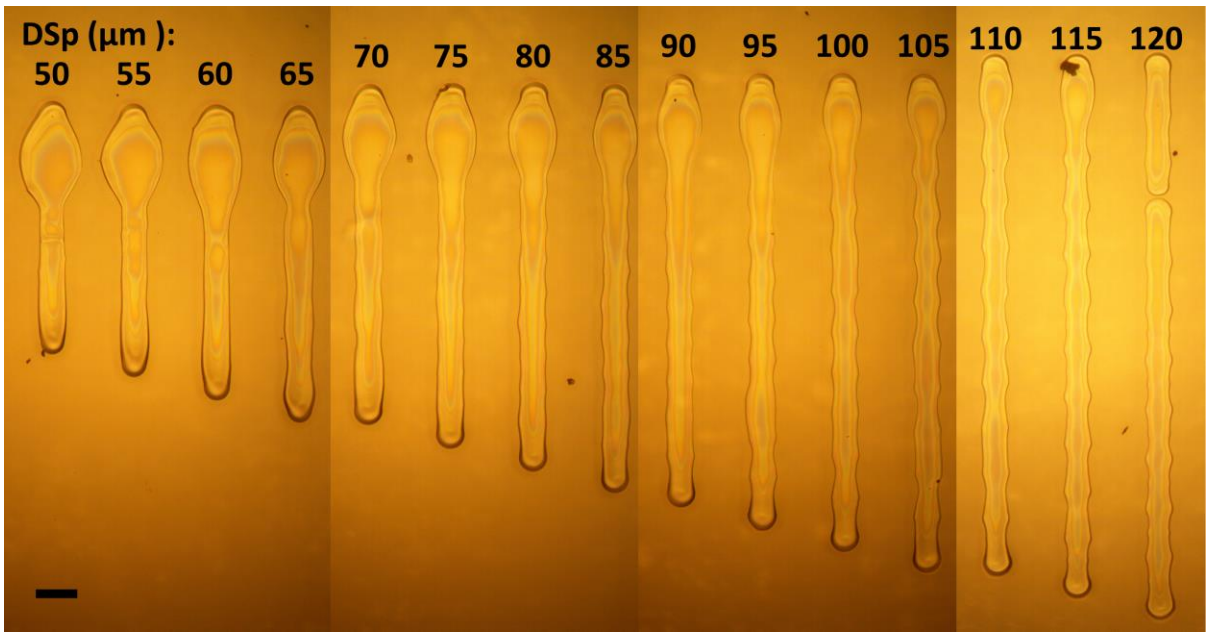


Fig. 4: PVP lines printed in a linear fashion with varying drop spacing. Bulging is clearly visible at the start of lines (top) with small drop spacing. Scalloping is also clearly visible for large values of drop spacing. The two regimes overlap. The only line without any bulging exhibits line separation (DSp=120$\mu$m). Scale bar represents 200$\mu$m.

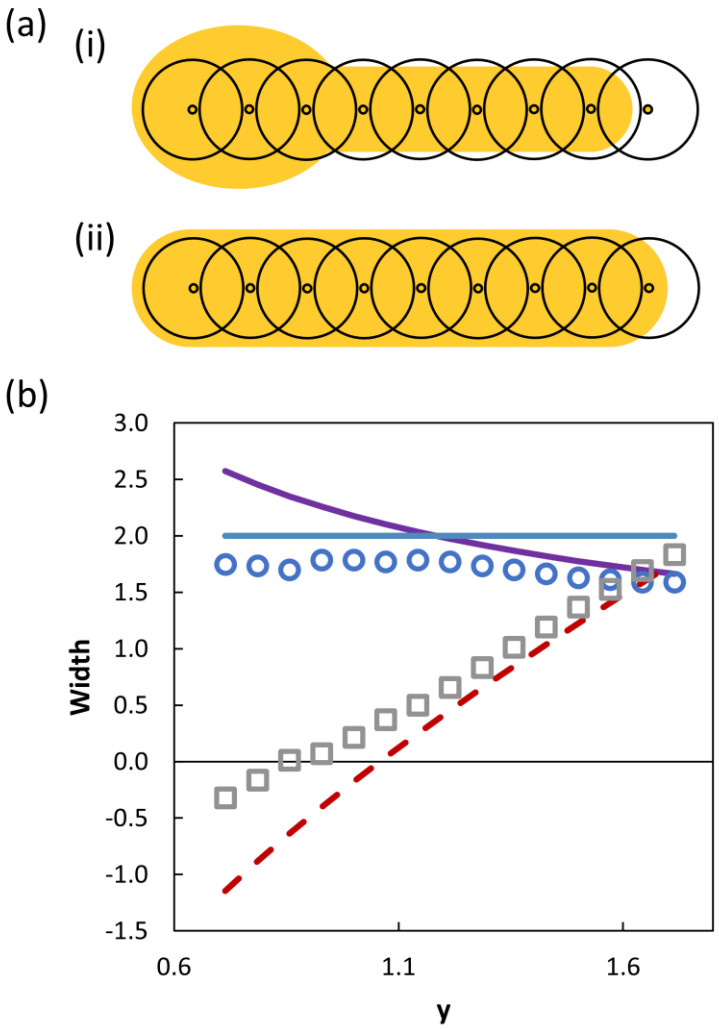


Fig. 5: (a) Illustration of scalloping mechanism induced by bulging. (i) With a bulge at the start of the line, ink is removed from the line reducing linewidth. Newly added drops land outside of the existing line and spread before merging with the line leading to scalloping. (ii) Without bulge for the same drop spacing, linewidth is larger. New drops land directly on the existing line preventing scalloping. (b) Stability diagram to identify drop spacing below which no scalloping occurs. Both axes show dimensions normalized by $R_S$. Stringer's model predicts this transition at the crossing point of the predicted line width (solid line) and the diameter of an isolated drop (horizontal line). However, experimental linewidth (circles) is less than the predicted value due to ink being removed to the bulge. Soltman's model considers where the diameter of impinging drops crosses zero as they make contact with the line. This gives good agreement with experimental values (transition at $y$=0.86) when the impinging diameter is calculated using experimental (squares) rather than predicted (dashed line) linewidth.

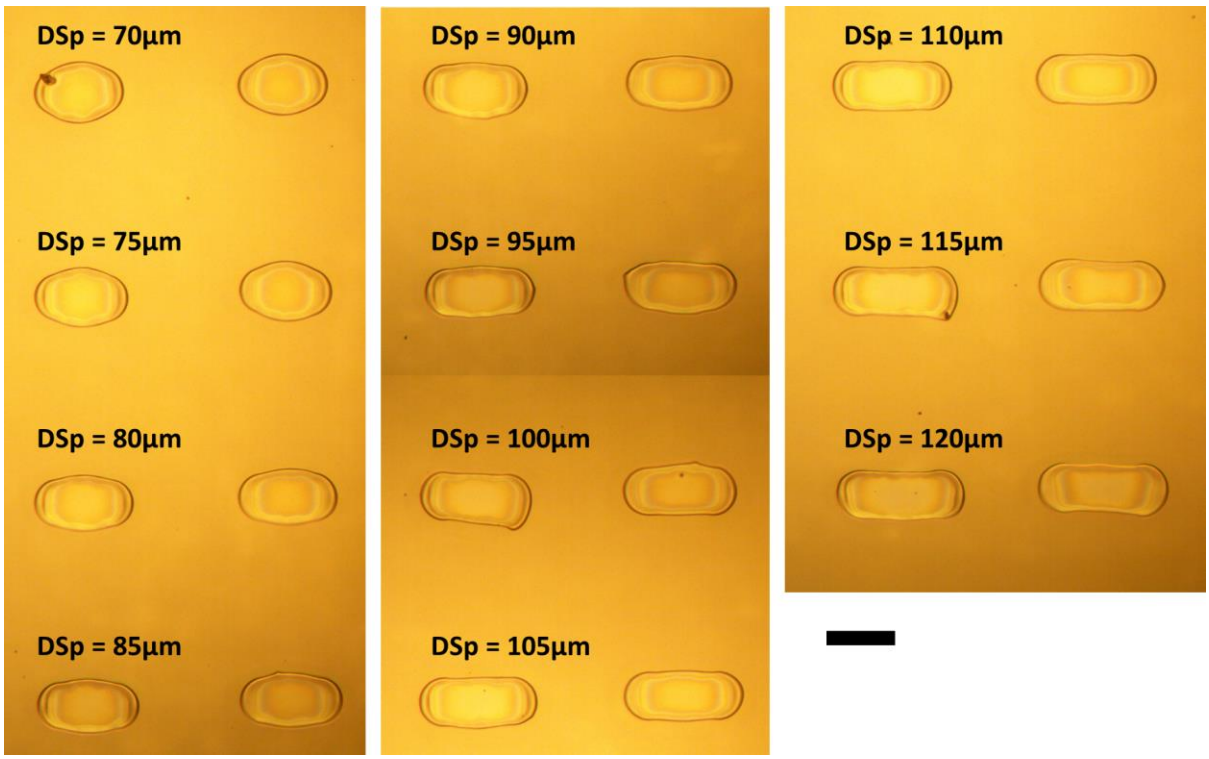


Fig. 6: Segments of three PVP drops printed symmetrically with varying drop spacing. Scale bar represents 200$\mu$m.

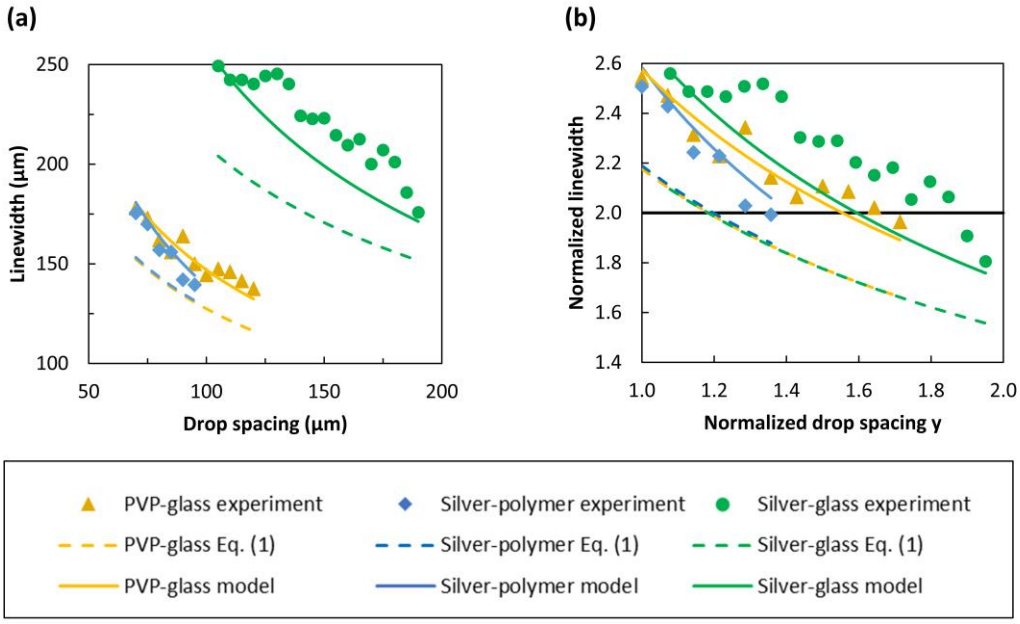


Fig. 7: Linewidth at the center of three-drop segments printed symmetrically as a function of drop spacing for three different ink-substrate systems. (a) absolute dimensions and (b) dimensions normalized by drop radius on substrate. Optimum drop spacing corresponds to segments with linewidth just above twice the drop radius (horizontal line in (b)).

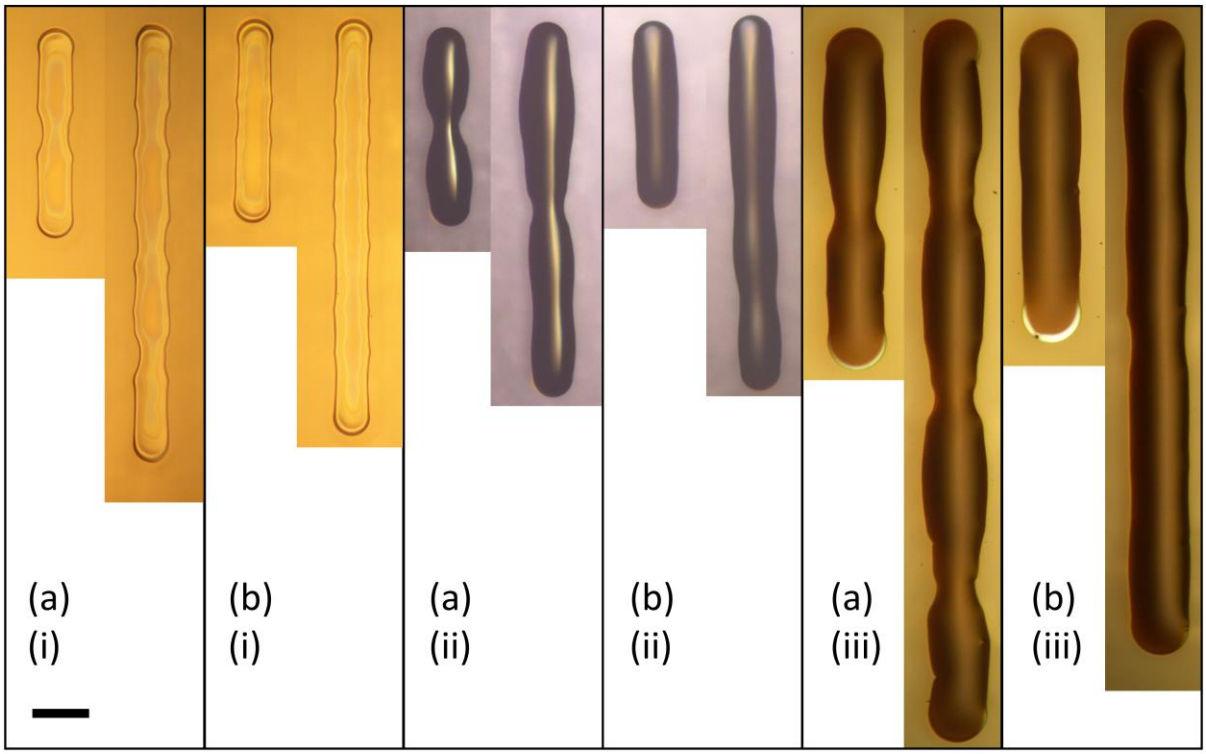


Fig. 8: Symmetrically printed lines with two (left) and four (right) segments. No bulging is observed. (a) Connecting drop spacing between segments is the same as drop spacing within segments. (b) Connecting drop spacing is reduced to minimum, significantly reducing scalloping. (i) PVP on glass. (ii) Silver on polymer. (iii) Silver on glass. Scale bar represents 200$\mu$m.

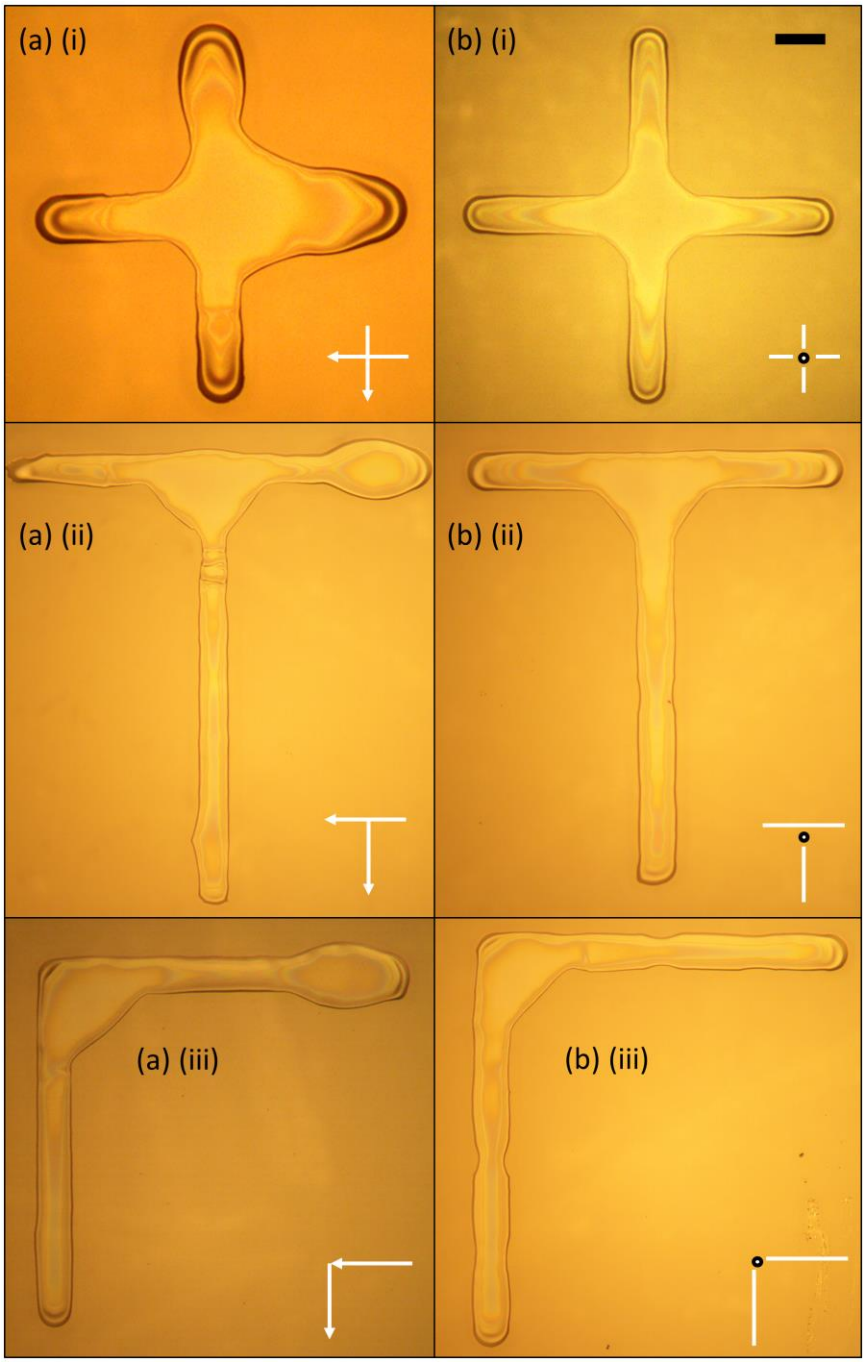


Fig. 9: X-, T- and L-shapes printed with (a) traditional linear method and (b) segmented and symmetric method without bulging. Insets illustrate printing methodologies. PVP on glass. Scale bar represents 200$\mu$m.

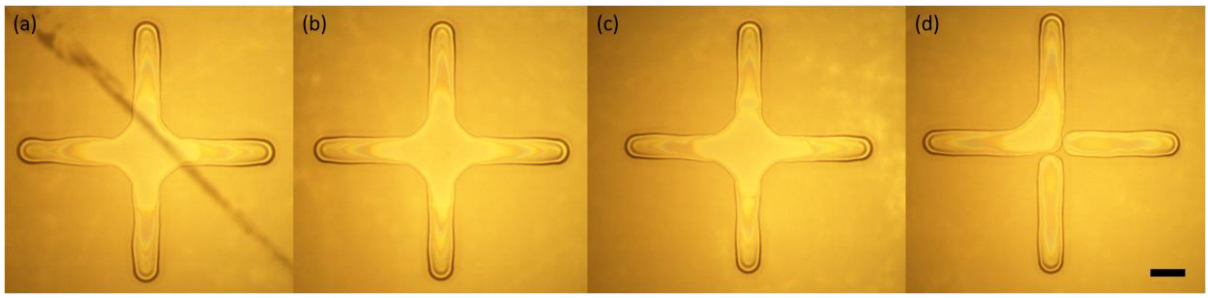


Fig. 10: X-shapes symmetrically printed with varying spacing between legs. The spacing between the center of the innermost drop in each segment and the center of the central connecting drop is (a) 110$\mu$m (b) 120$\mu$m (c) 130$\mu$m and (d) 140$\mu$m. PVP on glass. Scale bar represents 200$\mu$m.

| **Ink** | PVP | Silver | |
|---|---|---|---|
| **Substrate** | Display glass | Glass slide | PVP polymer |
| **Drop radius in air $R_0$ ($\mu$m)** | 30 | 37.75 | |
| **Drop volume $V_{drop}$ (pL)** | 113 | 225 | |
| **Drop radius on substrate $R_S$ ($\mu$m)** | 70 | 97 | 70 |
| **Contact angle $\theta$** | 23.4° | 17.5° | 43.4° |

Table 1: Measured properties of droplets in air after being ejected from nozzle and at interface with substrate